Heliyon 10 (2024) e29391

Contents lists available at ScienceDirect

Heliyon

journal homepage: www.cell.com/heliyon

Research article

Atmospheric corrosion of carbon steel: Results of one-year exposure in an andean tropical atmosphere in Colombia

Ana C. Santa [a,*], Diego A. Montoya [b], Jose A. Tamayo [a], Maryory A. Gómez [b], Juan G. Castaño [b], Libia M. Baena [c]

[a] Grupo Calidad Metrología y Producción, Instituto Tecnológico Metropolitano –ITM-, Medellín, Antioquia 050034, Colombia
[b] Centro de Investigación, Innovación y Desarrollo de Materiales – CIDEMAT, Facultad de Ingeniería, Universidad de Antioquia UdeA, Calle 70 No 52 – 21, Medellín, Colombia
[c] Grupo Química Básica, Aplicada y Ambiente – Alquimia, Facultad de Ciencias Exactas y Aplicadas, Instituto Tecnológico Metropolitano, Medellín, Antioquia, 050034, Colombia

ARTICLE INFO

Keywords:
Atmospheric corrosion
Carbon steel
Tropical atmosphere
Corrosion rate

ABSTRACT

In this study was examined the response of carbon steel to atmospheric corrosion after one-year exposure in Valle de Aburrá, a subregion located in northwestern Colombia. The study involved the assessment of material mass loss and corrosion rate, the characterization of atmospheric aggressiveness, and the analysis of the morphology and composition of corrosion products in five different sites. Climatological and meteorological factors were assessed by testing for chloride content, sulfur dioxide levels, and time of wetness (TOW). The analysis of corrosion products was conducted using scanning electron microscopy (SEM), X-ray diffraction (XRD), and Raman spectroscopy. Based on corrosion rates, two sites exhibited a more aggressive environment, with a corrosivity category of C3, while the remaining sites were categorized as C2. The study confirmed the presence of lepidocrocite and goethite phases on the surface of carbon steel at all test sites. Data analysis revealed that both the TOW and the industrial activity significantly influence the corrosion of this metal.

1. Introduction

Structural materials damage due to corrosion processes results in high building maintenance and rehabilitation costs [1,2]. Many metallic equipment and structures operate in the atmospheric environment, which poses an enormous challenge in corrosion science [3,4].

The corrosion process involves numerous site-specific variables, including the Time of Wetness (TOW), which is influenced by meteorological factors such as temperature and relative humidity. In addition, the presence of atmospheric elements such as SO_2 and chlorides accelerates atmospheric corrosion [5–7]. It is well known that corrosion rates of metals in the atmosphere may vary by tens or even hundreds of times depending on their location [8]. Hence, conducting corrosion studies specific to certain areas or regions is crucial [9].

Valle de Aburrá, located in the southern part of the Colombian department of Antioquia, in the heart of the Central Andes Cordillera, is a metropolitan area with distinctive geographical, meteorological, and urban growth characteristics that exacerbate air

* Corresponding author. Facultad de ingeniería, Instituto Tecnológico Metropolitano –ITM, Medellín, Antioquia, Colombia.
E-mail address: anasanta304720@correo.itm.edu.co (A.C. Santa).

https://doi.org/10.1016/j.heliyon.2024.e29391
Received 18 January 2024; Received in revised form 5 April 2024; Accepted 8 April 2024
Available online 9 April 2024

quality issues. It is affected by both stationary and mobile sources of pollution throughout its entire territory and is surrounded by towering mountains that impede air circulation during specific periods of the year.

Remarkably, the last atmospheric corrosion study in the city dates back sixteen years [6]. Therefore, analyzing the valley atmosphere's corrosivity evolution in recent years and assessing the impact of varying environmental factors is crucial to estimate the lifetime of carbon steel structures and equipment. Moreover, it aids in developing effective strategies to control corrosion.

In this study, atmospheric corrosion of carbon steel AISI - SAE 1005 and its susceptibility to different atmospheric variables were evaluated over a one-year period at five test stations within Valle de Aburrá. Corrosion products were characterized using Scanning Electron Microscopy (SEM), Energy Dispersive X-Ray Spectroscopy (EDS), X-Ray Diffraction (XRD), and micro-Raman Spectroscopy (RS).

2. Materials and methods

2.1. Materials

In this research was used carbon steel (CS, AISI/SAE 1005), a material commonly employed in construction applications. The CS samples were cut to dimensions of 10 × 12 × 0.1 cm, labeled with nylon thread for identification, subjected to sandblasting, and cleaned with absolute ethanol. The initial weights of all samples were recorded before exposing them to various sites in Valle de Aburrá for comparative analysis, in accordance with ASTM G31 (Section 7.9). Subsequently, the samples were sealed in airtight bags for transportation. Table 1 shows the chemical composition of CS, which was determined using a Bruker Q8 MAGELLAN optical emission spectrometer.

2.2. Exposure sites and sample assembly

The study was conducted in Valle de Aburrá, a region located in the department of Antioquia, in northwestern Colombia (see Fig. 1a). The five chosen locations were assigned the following notations: Site 1 - S1 (Center), Site 2 - S2 (West), Site 3 - S3 (Southeast), Site 4 - S4 (North), and Site 5 - S5 (Southwest). The carbon steel plates were placed on unprotected racks at an inclination of 60° facing north, according to ASTM G50 [10], as depicted in Fig. 2.

2.3. Determination of atmospheric pollutants and time of wetness (TOW)

Both sulfate and chloride collectors, prepared according to NBR-6921 and NBR-6211 standards, respectively, were used at the five test sites [11,12]. Additionally, CEM thermohydrometers (with a precision of ±5 % and ±2 °C) were employed to obtain continuous temperature and relative humidity readings. Using this dataset, time of wetness (TOW) was determined, defined as the fraction or percentage of time (monthly or yearly) during which the temperature surpasses 0 °C while the relative humidity equals or exceeds 80 % [13].

The quantification of chlorides and sulfates was performed using a METROSEP IC ion-exchange chromatograph (model 761 COMPACT IC, version 2.761.0020), on a quarterly basis until the end of the assessment. The level of atmospheric aggressiveness was determined following ISO 9223 guidelines. Fig. 1b shows the design of the pollutant collectors used in the corrosion stations.

2.4. Determination of mass loss and corrosion rates

The samples were exposed to the atmosphere for one year. Mass loss was measured, and corrosion rates were calculated on three replicates after 3, 6, 9, and 12 months of exposure. To determine mass loss, corrosion products were removed by chemical pickling according to Section 9 of ASTM G1 [14]. Afterward, the samples were washed with ethanol and dried using cold air. Weight data were recorded for each CS sample at each point (3, 6, 9, and 12 months). The corrosion rate was determined by measuring the mass loss, as shown in Equation (1), following the procedure outlined in Section 8.1 of ASTM G1.

$$r_{corr} = \frac{K * W}{A * t * \rho} \tag{1}$$

Where.

K = (8.76 x 10^4) is a constant
W = mass loss (g)

Table 1
Chemical composition of carbon steel (CS).

	Chemical composition (%)							
Fe	C	Si	Mn	P	S	Cr	Mo	Al
99.55	0.054	0.0034	0.256	0.0083	0.0051	0.023	0.0032	0.051

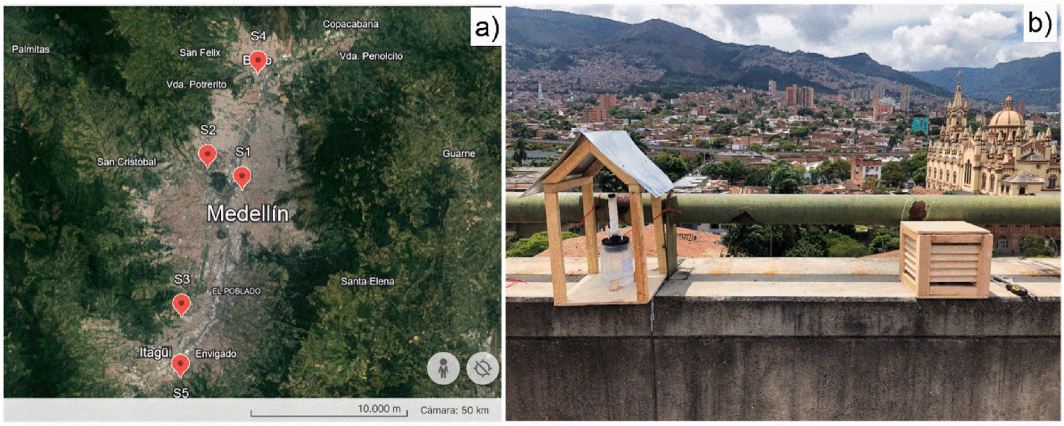

Fig. 1. a) Location of test sites in Valle de Aburrá, Colombia (Google earth) b) Sulfates and chlorides candles installed at S1.

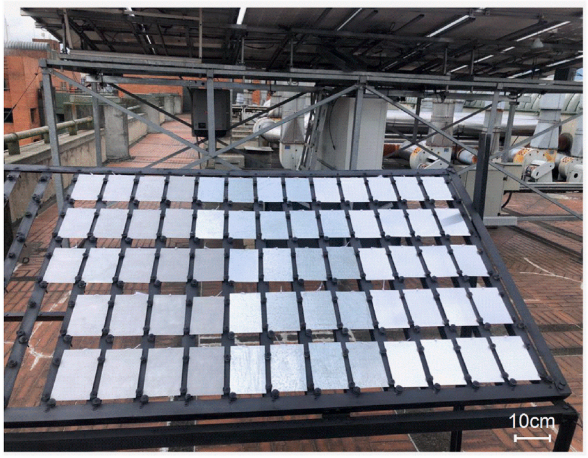

Fig. 2. Atmospheric exposure of CS samples.

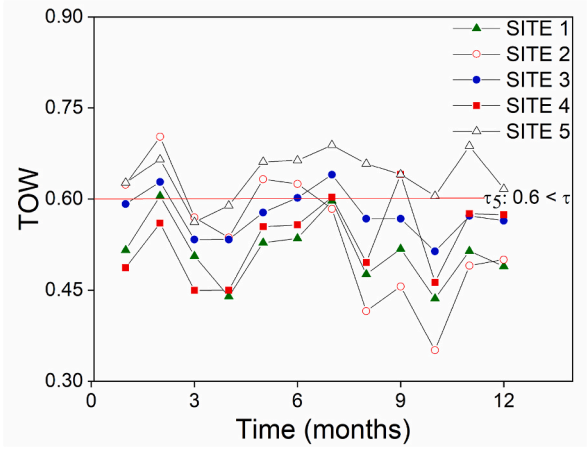

Fig. 3. Time of wetness (TOW) at each exposure site. TOW was higher at Sites 5 and 3.

A = area (cm^2)
T = time of exposure (hours)

$$P = \text{density}\ \left(g / cm^3\right)$$

2.5. Identification of corrosion products

Corrosion products were characterized at the end of the test. A JEOL JSM-7100 scanning electron microscope coupled with an Oxford X-Max EDS AZtec 51-XMX1178 energy dispersive system was used to analyze their morphology and composition both on the surface and in cross sections.

The characterization of the corrosion products' composition was complemented using a HORIBA Jobin Yvon LabRAM HR high-resolution confocal Raman spectrometer and a Malvern Panalytical Empyrean 2012 X-ray diffractometer equipped with a Pixel 3D detector and a Cu source (α = 1.541 Å) at 45 kV and 40 mA, with a step size of 0.02° and a dwell time of 46 s.

3. Results and discussion

3.1. Environmental characteristics of exposure sites

TOW was consistently high across all sites, as shown in Fig. 3. At exposure sites S1, S2, S3, and S4, the TOW fell into category ⁞4, while exposure site S5 was classified in category ⁞5, according to ISO 9223 [15]. Both TOW categories are high, favoring the formation of a sufficiently thick moisture layer on the steel substrate that allows the electrochemical corrosion reactions in anodic and cathodic zones most of the time [9]. Conversely, the rate of chloride deposition is negligible and has little impact on the process. However, at certain sites, sulfate deposition significantly contributes to the corrosion process alongside other variables.

In a study conducted between 2017 and 2018 in urban environments, Vidal et al. [4] reported high relative humidity values, where the TOW category for three corrosion stations was ⁞4. However, the corrosion rate for grey cast iron was found to be between 13 and 17 μm/year, which is lower than that obtained in this study for CS, except for S2. This difference could be attributed to the higher amount of sulfates observed in the present study, as shown in Table 3. Moreover, Vidal and colleagues reported a decrease in acid contamination compared to previous studies conducted in the same location.

Table 2 indicates that the TOW was greater than 4500 h/year for all test sites. Fig. 3 depicts a TOW behavior typical of tropical regions [7]. Particularly, Valle de Aburrá is classified as a humid tropical zone and has been experiencing unexpected increases in rainfall in recent years. As observed in Fig. 3. December, January, and February experienced the lowest TOW, corresponding to months 8 through 10. This is consistent with findings from various studies [16–18], which indicate a period of low rainfall during these months followed by a second dry season from July to August (months 2 through 4).

The areas located in the southern part of Valle de Aburrá exhibited the highest TOW, although this variable also remains notably high in the other areas.

Monthly chloride and sulfate deposition are illustrated in Fig. 4a and b respectively. S3 and S4 exhibited the highest rates of chloride deposition; however, they were minimal across all sites. Similarly, sulfate deposition remained below 70 mg/m^2.day in most measured periods and at all stations, except for an increase in January 2023 (month 9), which was noticeable for S4, significant for S5, and moderate for S3.

Table 3 presents the environmental pollution variables measured at the five test stations, as well as an atmospheric categorization based on ISO 9223.

The SO_2 deposition rates measured at S1, S2, S3, and S5 fall within the P0 ISO 9223 category, while S4 is classified under the P1 category. Considering this, it can be determined that S4 exhibits the highest SO_2 deposition rate, followed by S5, and the three sites located in industrial areas. Accordingly, this atmosphere has low chloride and moderate sulfate contents. Sulfate deposition rates lower than 10 mg/m^2 d correspond to rural atmospheres, between 10 and 100 mg/m^2.d correspond to urban atmospheres, and higher than 100 mg/m^2.d correspond to industrial atmospheres [19,20].

3.2. Sample mass loss and corrosion rate

Fig. 5 displays the variation in mass loss of CS at the five exposure sites until the end of the test. The order of mass loss was S4 > S3 > S1 > S5 > S2. Presumably, S4 (north) exhibited the highest mass loss due to high SO_2 content and TOW levels. Furthermore, this

Table 2
Time of wetness per year for the five test sites. Category assigned according to ISO 9223.

Site	TOW (hours/year)	Category
S1	4499.23	⁞4
S2	4743.13	⁞4
S3	5032.28	⁞4
S4	4588.35	⁞4
S5	5595.54	⁞5

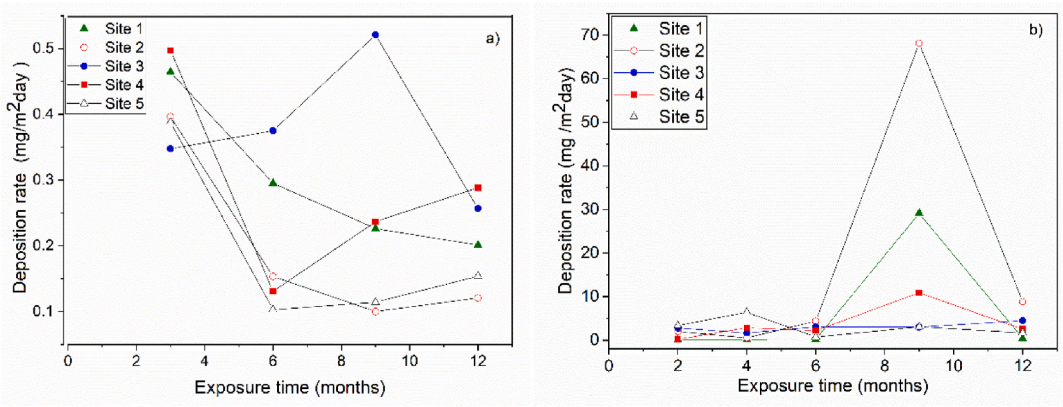

Fig. 4. Deposition rates at the five test sites for various exposure periods. a) Cl^- deposition; b) SO_2 deposition.

Table 3
Environmental pollution variables, climatic features, and pollution data obtained by ion chromatography.

Site	Deposition rate SO_2 (mg/m^2.d)	P	Deposition rate Cl^- (mg/m^2.d)	S	TOW (hours/year)	ł	CA
S1	2.3954	P0	0.2968	S0	4499.23	ł4	3
S2	2.4399	P0	0.1928	S0	4743.13	ł4	3
S3	3.7265	P0	0.4999	S0	5032.28	ł4	3
S4	16.7838	P1	0.3843	S0	4588.35	ł4	3
S5	5.9865	P0	0.1898	S0	5595.54	ł5	3 or 4

P, S, ł: Categories for SO_2, Cl^-, and TOW, respectively. CA: Corrosivity category. (Environmental parameters according to ISO 9223).

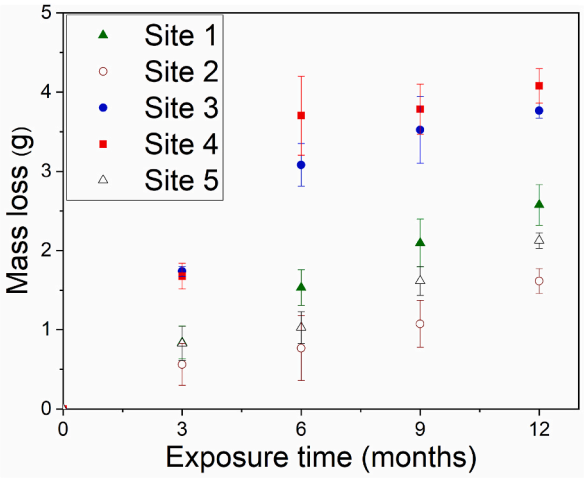

Fig. 5. Mass loss of carbon steel over one year of exposure in Valle de Aburrá.

Table 4
Categorization of atmospheric aggressiveness.

Site	Vcorr (μm/y)	CA
	AC	AC
Site 1	21.88	C2
Site 2	13.73	C2
Site 3	31.98	C3
Site 4	34.65	C3
Site 5	18.06	C2

station is located near a highway with heavy traffic. This figure also shows a cumulative mass loss trend for all sites, highlighting a stabilization at S3 and S4. This phenomenon demonstrates the protective capacity of the corrosion products that form on the metal. Moreover, S3 and S4 experienced a higher mass loss, explained by their location in industrial areas with high pollution levels and presence of particles from metal cutting and organic paints, as well as longer TOW.

TOW and sulfate deposition rate have an impact on mass loss at sites with both industrial atmosphere and tropical humidity characteristics. A study conducted in tropical areas [21] reported high TOW and ł4 categories at three sites. The sulfate concentrations at one of the study sites (St John's Island, 16.9 mg/m^2.d) are consistent with those observed in this study. At the same station, the mass loss was 237 g/m^2 and the corrosivity category was C3, which is consistent with the mass losses found at sites S3 (314 g/m^2) and S4 (340 g/m^2) in this study (see Fig. 5).

Table 4 shows the corrosion rate of CS at each of the study stations. S4 exhibited the highest corrosion rate, followed by S3. According to ISO 9223, the corrosivity categories of the sites evaluated in this study were C2 and C3. Similar findings have been identified in studies in urban and industrial exposure sites. For example, Zafar et al. [22] reported C3 corrosivity categories for corrosion stations in urban and industrial areas with chloride and sulfate contents higher than those found in the present study. The sulfate contents had minimum values of 88 mg/m^2.d, and maximum values of 190 mg/m^2.d. However, the average TOW was 2000 h/year, which is lower than that found in this research. Similarly, Correa et al. [6] conducted a study on Colombian atmospheres in 2007 and found that the values for mass loss and sulfate contents in urban stations were comparable to those in this study.

In the course of one year, S3 and S4 displayed a corrosion rate of approximately 35 μm/year, whereas S1, S2, and S5 achieved values ranging from 22 to 14 μm/year. Another study conducted in 2010 on atmospheric corrosion at six sites in Colombia, including Medellín (which is part of Valle de Aburrá), the corrosion rate was 25.93 μm/year. This rate is higher than that of S1, S2, and S5, but lower than that of S3 and S4 [6]. However, in both cases, the aggressiveness category of the Medellín environment for CS is still C2 and C3 (moderate) according to ISO 9223.

Comparisons were made between the corrosion rates obtained in this study and those reported by other authors with similar corrosion categories (see Fig. 6). It is noteworthy that all these sites fall within the classification of urban or industrial-urban atmospheres [6,23–29].

Fig. 6 show the corrosion rate observed in this study aligns with findings from various authors documenting corrosion rates at other sites. However, it is noteworthy that the sulfate deposition levels in our study are notably lower compared to those reported by different authors for similar corrosion rates at their respective sites.

According to the data in Fig. 6, the increase in SO_2 content has a moderate influence on the corrosion rate. This may be due to the formation of protective layer of corrosion products, as evidenced in other studies [6]. Without ignoring the effect of SO_2, other factors such as TOW could have a prominent role in this type of atmospheres.

Observing atmospheric conditions categorized as industrial-urban and urban, it is evident that sites 3 and 4 in this investigation exhibit corrosion rates similar to Zaragoza, Spain [23], Beijing, China [24] and Sendai, Japan [25]. These rates surpass those of other reported sites. Conversely, site 1 in this study manifests a corrosion rate positioned at a midpoint, comparable with other sites as Hanoi (Vietnam) [26]. Sites 2 and 5 exhibit corrosion rates at the lower end of the spectrum reported for such atmospheres; however, it is worth noting that these values have also been reported by other authors [6,27–29].

The corrosivity categories determined by environmental parameters are somewhat different from those determined by corrosion rates. Although no direct relationship is observed between chloride deposition, sulfate deposition, TOW, and mass loss, high relative humidity percentages appear to have an impact on the corrosion process. Particularly, S4 experienced greater pollutant deposition, resulting in higher mass losses and corrosion rates. The high mass losses at S4 and S3 are related to the industrial activity in these areas.

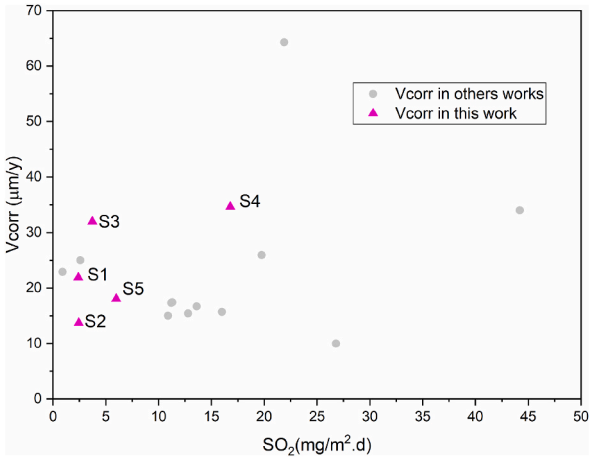

Fig. 6. Corrosion rates vs sulfate deposition for the stations including in this study and those reported by other authors in urban and industrial-urban atmospheres.

3.3. Characterization of corrosion products

3.3.1. Raman spectra

Fig. 7 displays the Raman spectra for the CS samples tested during one year at each exposure site. These spectra exhibit bands that resemble iron oxides often found in steel corrosion products. Peaks at 252, 1302, and 650 cm^{-1} suggest the existence of lepidocrocite (γ-FeOOH). On the other hand, peaks at 300, 379, and 650 cm^{-1} are indicative of the existence of goethite (α-FeOOH) [30].

The Raman spectra of iron oxides and hydroxides demonstrate visible bending of the Fe–*O*–H group and stretching of the Fe–O group within the 1200–600 cm^{-1} region. Overlapping bands and molecular frequencies are observed in the 600–200 cm^{-1} region, as reported in previous research [31]. Table 5 shows the peaks corresponding to the oxyhydroxides found in different studies, where * is the prominent band [31–33]. Table 6 shows the peaks found for each of the exposure sites, where * are the most prominent bands in the corrosion products found in this study.

At all five exposure sites, lepidocrocite was observed to be the primary corrosion product based on the high peak intensity at 250 and 377 cm^{-1}, which is consistent with previous studies [24,26–28]. Rust analysis also revealed a combination of lepidocrocite and goethite, with the most representative bands at 245, 299, 385, 479, and 550 cm^{-1}. The spectral analysis provides a distinct differentiation between goethite and lepidocrocite, despite significant overlapping of bands, particularly at the 245 cm^{-1} region.

3.3.2. X-ray diffraction

The corrosion products formed at the five exposure sites were analyzed using XRD (Fig. 8). The samples collected from all the sites showed the presence of the same main components: lepidocrocite (γ-FeOOH) and goethite (α-FeOOH), which is consistent with the findings of previous studies [6,21,29–31].

The typical peaks for lepidocrocite were observed at 2Θ values of 14°, 37°, 53°, 60°, with 27° being the main peak. Several consecutive peaks were observed at 34° and between 38° and 41° for goethite [27,28].

According to the XRD results, lepidocrocite was the main corrosion product. Additionally, a broad diffraction peak at 21.3° indicated the presence of goethite, albeit in small amounts. At S3, goethite was also observed at 34.6°.

3.3.3. Scanning electron microscopy and energy-dispersive X-ray spectroscopy

Figs. 9–13 display SEM images of the morphology of the corrosion products after one-year exposure. Fig. 9a shows the presence of lepidocrocite on steel at S1. Specific morphological characteristics of lepidocrocite, and in some instances goethite, were observed at all sites. Floral and plate crystals typical of lepidocrocite and cotton ball structures common to semi-crystalline goethite samples [6,22] were easily identified in all samples. None of the analyzed samples exhibited the magnetite pattern, which consists of flat, dark patches with round disks [34].

Fig. 9a and b shows lepidocrocite in the form of plates. According to Seechurn et al. [35], these plates of lepidocrocite emulate the form of tree roots and tentacles. Similarly, lepidocrocite plates are observed in Fig. 10a and c, however, according to Fig. 10b, goethite cotton balls can be observed at low magnifications.

Fig. 11(a–c), the characteristic structure of lepidocrocite is evident, albeit at a magnification of 10.000×, where its appearance is notably finer. The finely structured lepidocrocite is also discernible in Fig. 12a and b, alongside globular formations of the same observed in Fig. 12c. The "strings" observed at S5 in Figs. 13a and b represent structures made of lepidocrocite crystals, resembling strings, which had been previously detected in Colombian atmospheres [6]. Fig. 13c show lepidocrocite in the form of plates.

The predominance of goethite and lepidocrocite with the observed morphologies corresponds to initial states of atmospheric corrosion.

4. Conclusions

S4 (in the northern part of Valle de Aburrá) and S3 (in the southern area) exhibited the highest levels of aggressiveness, most likely due to their intense industrial activity. In contrast, the aggressiveness of remaining sites was associated with urban activity. The highest level of corrosivity at S4 can also be related to high industrial activity and the influence of a nearby highway. Similarly, the corrosivity at S3 is linked to its intensive industrial activity.

In all cases, the assessed sites displayed a corrosivity level ranging from slightly high (C3) to moderate (C2). Compared to previous studies conducted in Valle de Aburrá more than 15 years ago, the SO_2 deposition rate is slightly low at S4, where the highest level of aggressiveness is recorded. However, the corrosivity level has not changed significantly.

The findings derived from studies carried out in atmospheres with analogous conditions have demonstrated the importance of sulfate content and TOW to the corrosion process. These findings bear substantial implications for the design and selection of materials for applications involving exposure to corrosive atmospheres. It is imperative to carefully consider the concentration of sulfate present in the environment, as well as the duration of exposure to moisture when selecting materials and establishing appropriate maintenance protocols.

Aggressivity categories revealed discrepancies between environmental parameters and corrosion rates. Following the classification based on corrosion rate, CS exhibited a lower category if compared to classification based on environmental factors. However, it is important to assess both environmental parameters and corrosion rates for a better assessment of materials' susceptibility.

The presence of only oxyhydroxides (lepidocrocite and goethite) in CS suggests initial stages of the corrosion process in all sites.

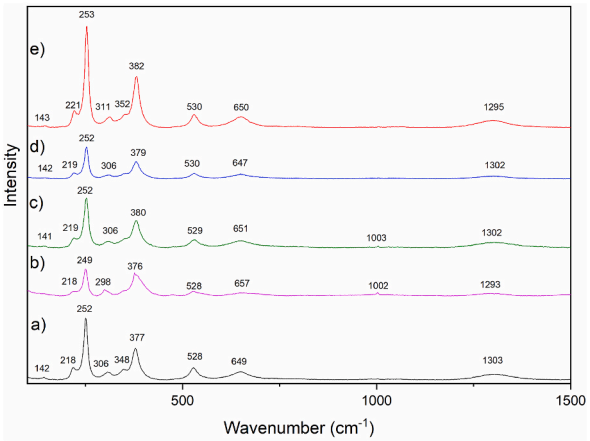

Fig. 7. Raman spectra of carbon steel after one year of exposure, showing lepidocrocite and goethite in the corrosion products at all exposure sites. a) S1, b) S2, c) S3, d) S4, e) S5.

Table 5
Raman spectra of the carbon steel corrosion products.

Corrosion product	Characteristic band (cm^{-1})				
Goethite	250	308	376*	525	644
Lepidocrocite	250*	376	524	644	

Table 6
Raman spectra of the carbon steel corrosion products at each site.

Site	Characteristic band (cm^{-1})									
Site 1	142	218	252*	306	348	377*	528	649		1303
Site 2		218	249*	298		376*	528	657	1002	1293
Site 3	141	219	252*	306		380*	529	651	1003	1302
Site 4	142	219	252*	306		379*	530	647		1302
Site 5	143	221	253*	311	352	382*	530	650		1295

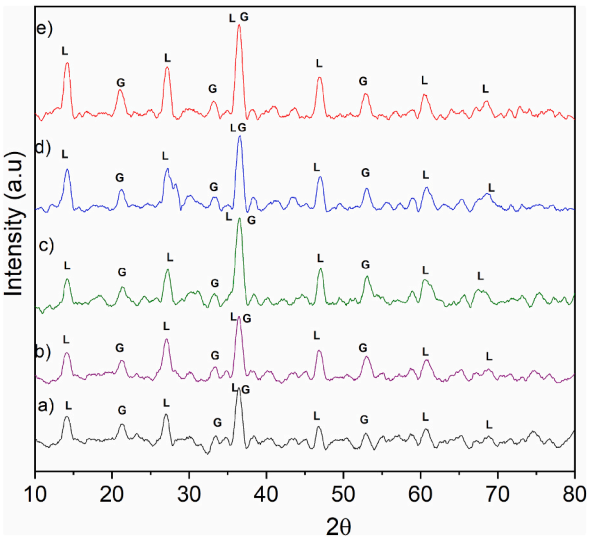

Fig. 8. XRD spectra of carbon steel after one year of exposure, showing lepidocrocite and a minor proportion of goethite in the corrosion products at all exposure sites. a) S1, b) S2, c) S3, d) S4, e) S5. L: lepidocrocite, G: goethite.

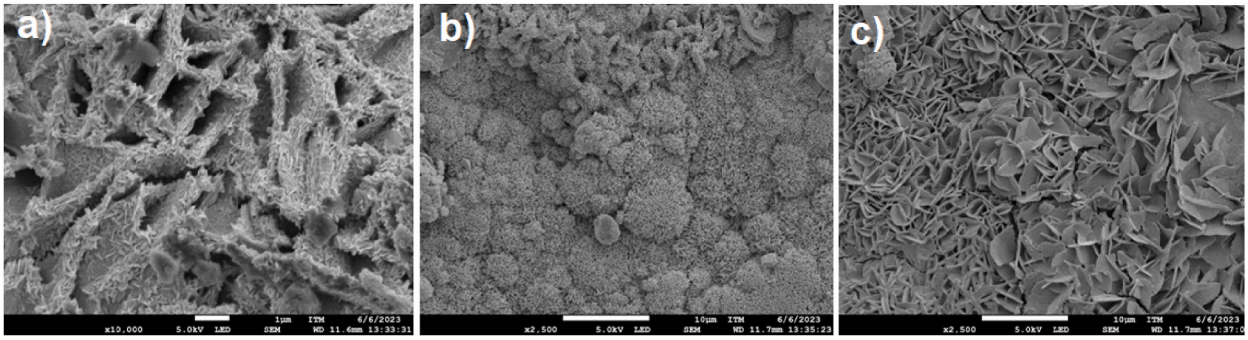

Fig. 9. SEM micrographs of the carbon steel rust surface layers at S1.

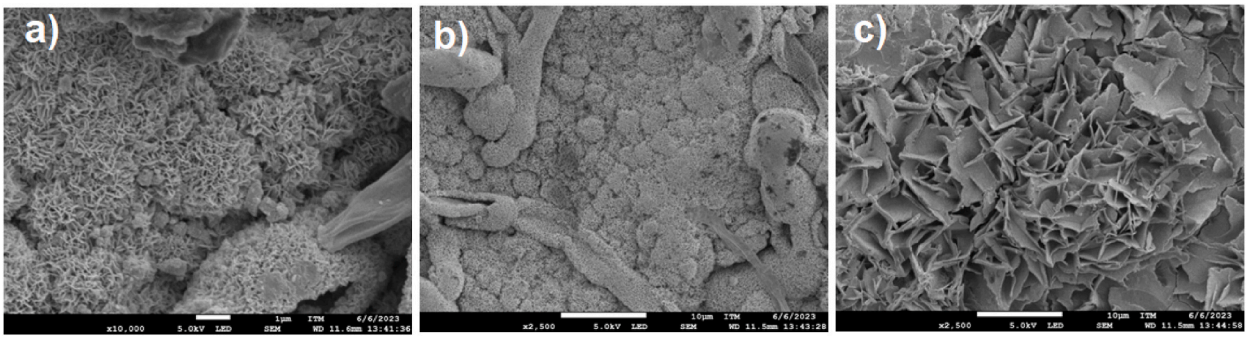

Fig. 10. SEM micrographs of the carbon steel rust surface layers at S2.

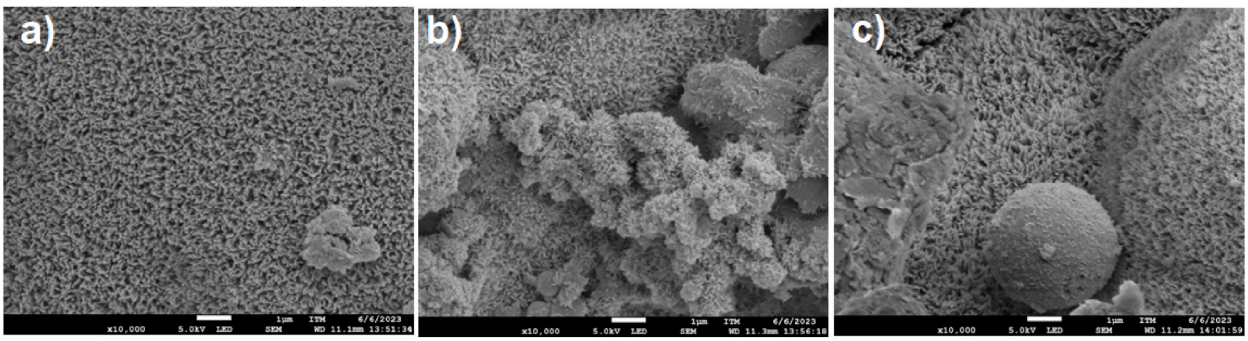

Fig. 11. SEM micrographs of the carbon steel rust surface layers at S3.

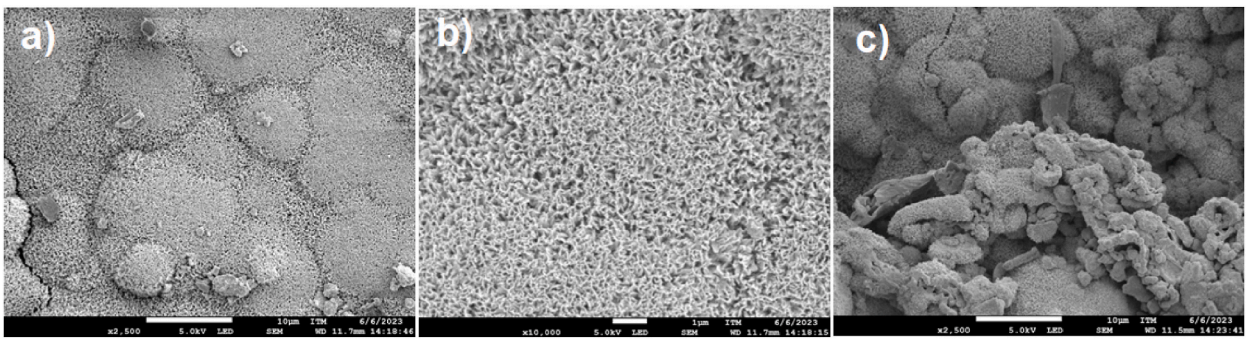

Fig. 12. SEM micrographs of the carbon steel rust surface layers at S4.

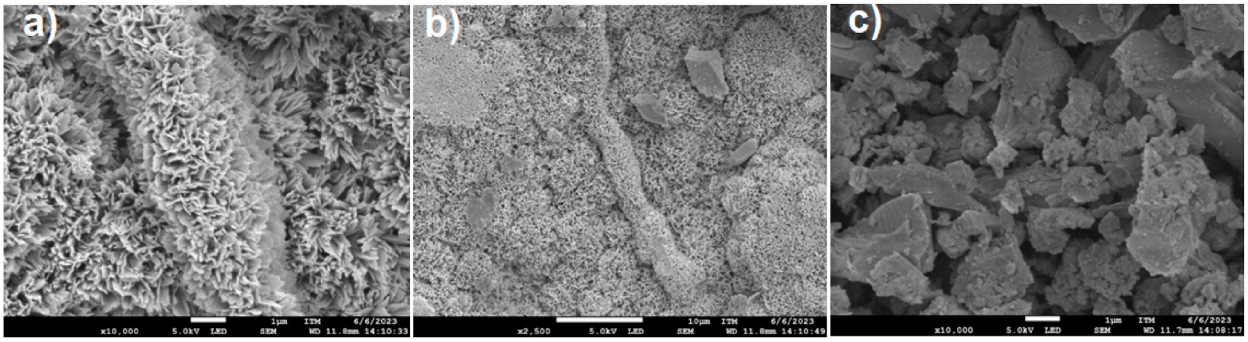

Fig. 13. SEM micrographs of the carbon steel rust surface layers at S5.

Data availability statement

Data associated with your study has not been deposited into a publicly available repository. Data will be made available on request.

CRediT authorship contribution statement

Ana C. Santa: Writing – original draft, Methodology, Investigation, Data curation. **Diego A. Montoya:** Formal analysis, Data curation. **Jose A. Tamayo:** Supervision, Project administration. **Maryory A. Gómez:** Writing – review & editing, Supervision, Conceptualization. **Juan G. Castaño:** Writing – review & editing, Visualization, Validation, Supervision, Investigation, Formal analysis, Conceptualization. **Libia M. Baena:** Writing – review & editing, Supervision, Resources, Project administration, Conceptualization.

Declaration of competing interest

The authors declare that they have no known competing financial interests or personal relationships that could have appeared to influence the work reported in this paper.

References

[1] M. Ivaskova, P. Kotes, M. Brodnan, Air pollution as an important factor in construction materials deterioration in Slovak Republic, in: Procedia Engineering, Elsevier Ltd, Jan. 2015, pp. 131–138, https://doi.org/10.1016/j.proeng.2015.06.128.
[2] A. Ghanbarzadeh, J. Neshati, M.R. Bagherzadeh, S. Ghanizadeh, Atmospheric corrosion map of an oil refinery, Anti-corrosion Methods & Mater. 60 (2) (2013) 106–114, https://doi.org/10.1108/00035591311308083.
[3] Annual atmospheric corrosion of carbon steel Worldwide. An Integration of ISOCORRAG, ICP/UNECE and MICAT databases, Materials 10 (6) (May 2017) 601, https://doi.org/10.3390/ma10060601.
[4] F. Vidal, R. Vicente, A.C. Bastos, A.M. Ferro Rocha, J. Mendes Silva, Atmospheric corrosion in two different urban environments in Portugal: results of one-year exposure, Corrosion Eng. Sci. Technol. 54 (7) (2019) 614–626, https://doi.org/10.1080/1478422X.2019.1646007.
[5] V. Krivy, M. Kubzová, K. Kreislova, V. Urban, Characterization of corrosion products on weathering steel bridges influenced by chloride deposition, Metals 7 (9) (2017) 16, https://doi.org/10.3390/met7090336.
[6] J.G. Castaño, C.A. Botero, A.H. Restrepo, E.A. Agudelo, E. Correa, F. Echeverría, Atmospheric corrosion of carbon steel in Colombia, Corros Sci 52 (1) (Jan. 2010) 216–223, https://doi.org/10.1016/j.corsci.2009.09.006.
[7] W. Pongsaksawad, et al., Atmospheric corrosion monitoring sensor in corrosion rate prediction of carbon and weathering steels in Thailand, Mater. Trans. 61 (12) (2020), https://doi.org/10.2320/matertrans.MT-M2020230.
[8] V. Kumar, N. Sharma, S.K. Tiwari, S. Kango, Atmospheric corrosion of materials and their effects on mechanical properties: a brief review, Mater Today Proc (Dec. 2020), https://doi.org/10.1016/j.matpr.2020.10.939.
[9] J. Morales, S. Martín-Krijer, F. Díaz, J. Hernández-Borges, S. González, Atmospheric corrosion in subtropical areas: influences of time of wetness and deficiency of the ISO 9223 norm, Corros Sci 47 (8) (Aug. 2005) 2005–2019, https://doi.org/10.1016/j.corsci.2004.09.005.
[10] A. International, ASTM G -50: Standard Practice for Conducting Atmospheric Corrosion Tests on Metals, vol. 76, 2010, pp. 1–5. Reapproved 2003.
[11] Norma Brasilera NBR-6921, Sulfatação total na atmosfera-determinação da taxa pelo método da vela de dióxido de chumbo, 1981.
[12] Brazilian Standards: ABNT, NBR 6211: Atmospheric Corrosion - Determination of the Chloride Deposition Rate in Atmosphere by Wet Candle Method, 2011.
[13] C. Leygraf, I.O. Wallinder, J. Tidblad, T. Graedel, Atmospheric Corrosion, Wiley, 2016, https://doi.org/10.1002/9781118762134.
[14] American society for testing materials ASTM, Astm G1-90: standard practice for preparing , cleaning , and evaluating corrosion test, Significance 90 (1999) 1–11. Reapproved.
[15] International Organization for Standardization (ISO), ISO 9223: Corrosion of Metals and Alloys- Corrosivity of Atmospheres-Classification, vol. 1, 1992.
[16] SIATA, "¿Qué se espera para el Valle de Aburrá en temporada de menos lluvias?," [en línea] https://siata.gov.co/sitio_web/index.php/noticia15. Medellín, July. 12, 2021.
[17] Gisel Guzmán Echavarría, Análisis de la influencia del diseño urbano en la meteorología del Valle de Aburrá [en línea], 2018 [Fecha consulta: 10 de febrero 2024].
[18] IDEAM, Caracteristicas climatológicas de ciudades y municipios turísticos, 2018. http://www.ideam.gov.co/web/tiempo-y-clima/clima [en línea] 2018 [Fecha consulta : 23 de enero 2024].
[19] S. Abdul-Wahab, C. Bakheit, S.A. Abdul-Wahab, C.S. Bakheit, R.A. Siddiqui, S.M. Al-Alawi, Atmospheric corrosion of metals, J. Corrosion Sci. Eng. 15 (10) (1968).
[20] C. Hai, et al., Analysis of corrosion evolution in carbon steel in the subtropical atmospheric environment of sichuan, J. Mater. Eng. Perform. (2021) 1–9, https://doi.org/10.1007/S11665-021-06019-1. Jul 2021.

[21] S. Wijesinghe, T. Zixi, Effect of tropical atmosphere on corrosion of different metals: corrosivity measurements of Singapore, ECS Meeting Abstracts 16 (6) (2015) 273–277, https://doi.org/10.1149/ma2015-02/11/630.
[22] F. Zafar, H. Bano, A. Mahmood, F. Corvo, J. Rodriguez, Physicochemical studies of mild steel corrosion and atmospheric corrosivity mapping of Karachi: an important harbor city of modern Maritime Silk Route, Mater. Corros. 71 (9) (2020) 1557–1575, https://doi.org/10.1002/maco.202011793.
[23] M. Morcillo, S. Feliu, S. Giménez, Long-term atmospheric corrosion of mild steel, zinc, copper and aluminium in Spain, Key Eng. Mater. 20–28 (Jan. 1991) 17–26, https://doi.org/10.4028/www.scientific.net/KEM.20-28.17.
[24] W. Hou, C. Liang, Eight-year atmospheric corrosion exposure of steels in China, Corrosion 55 (1999) 65–73. Available, https://api.semanticscholar.org/CorpusID:135977707.
[25] M. Yamashita, A. Maeda, H. Uchida, T. Kamimura, H. Miyuki, Crystalline rust compositions and weathering properties of steels exposed in nation-wide atmospheres for 17 years, J. Jpn. Inst. Metals 65 (11) (2001) 967–971, https://doi.org/10.2320/jinstmet1952.65.11_967.
[26] I. Cole, P. Corrigan, V.H. Nguyen, Steel corrosion map of vietnam, Corrosion Science and Technology 11 (4) (2012), https://doi.org/10.14773/cst.2012.11.4.103.
[27] J.F. Ríos-Rojas, D. Escobar-Ocampo, E.A. Hernández-García, C. Arroyave, Corrosividad atmosférica en Bogotá como metrópolis a una gran altitud, inquietudes a normas internacionales, DYNA (Colombia) 82 (190) (2015) 128–137, https://doi.org/10.15446/dyna.v82n190.46256.
[28] Z. Wang, et al., Atmospheric corrosion analysis and rust evolution research of Q235 carbon steel at different exposure stages in chengdu atmospheric environment of China, Scanning 2020 (2020), https://doi.org/10.1155/2020/9591516.
[29] M. Shiri, D. Rezakhani, Estimated and stationary atmospheric corrosion rate of carbon steel, galvanized steel, copper and aluminum in Iran, Metall Mater Trans A Phys Metall Mater Sci 51 (1) (2020) 342–367, https://doi.org/10.1007/s11661-019-05509-1.
[30] S. Das, M.J. Hendry, Application of Raman spectroscopy to identify iron minerals commonly found in mine wastes, Chem. Geol. 290 (3–4) (2011) 101–108, https://doi.org/10.1016/j.chemgeo.2011.09.001.
[31] M. Hanesch, Raman spectroscopy of iron oxides and (oxy)hydroxides at low laser power and possible applications in environmental magnetic studies, Geophys. J. Int. 177 (3) (2009) 941–948, https://doi.org/10.1111/j.1365-246X.2009.04122.x.
[32] J. Gui, T.M. Devine, In situ vibrational spectra of the passive film on iron in buffered borate solution, Corros Sci 32 (10) (1991) 1105–1124, https://doi.org/10.1016/0010-938X(91)90096-8.
[33] B.Y.R. Surnam, C.W. Chui, H. Xiao, H. Liang, Investigating atmospheric corrosion behavior of carbon steel in coastal regions of Mauritius using Raman Spectroscopy, Rev. Mater. 21 (1) (2016) 157–168, https://doi.org/10.1590/S1517-707620160001.0014.
[34] S. Fonna, I. Bin M. Ibrahim, Gunawarman, S. Huzni, M. Ikhsan, S. Thalib, Investigation of corrosion products formed on the surface of carbon steel exposed in Banda Aceh's atmosphere, Hel iyon 7 (4) (2021), https://doi.org/10.1016/j.heliyon.2021.e06608.
[35] Y. Seechurn, J.A. Wharton, B.Y.R. Surnam, Mechanistic modelling of atmospheric corrosion of carbon steel in Port-Louis by electrochemical characterisation of rust layers, Mater. Chem. Phys. 291 (Nov) (2022), https://doi.org/10.1016/j.matchemphys.2022.126694.